Research Square

Preprints are preliminary reports that have not undergone peer review.
They should not be considered conclusive, used to inform clinical practice,
or referenced by the media as validated information.

Photonic Topology Optimization with Thermomechanical Coupling from a Unified Variational Framework

Sebastian Wolf

wolf@ikm.uni-hannover.de

Philipp Junker

Research Article

Keywords:

Posted Date: November 20th, 2026

DOI: https://doi.org/10.21203/rs.3.rs-10358226/v1

License: This work is licensed under a Creative Commons Attribution 4.0 International License.
Read Full License

Additional Declarations: No competing interests reported.

Photonic Topology Optimization with Thermomechanical Coupling from a Unified Variational Framework

Sebastian Wolf[1], Philipp Junker[1]
1: Leibniz University Hannover, Institute of Continuum Mechanics, An der Universität 1, 30823 Garbsen
☎ (+49) 511 762 4120
✉ wolf@ikm.uni-hannover.de, junker@ikm.uni-hannover.de

Acknowledgements

This work is supported by the Deutsche Forschungsgemeinschaft (DFG) under Germany's Excellence Strategy within the cluster of Excellence PhoenixD (EXC 2122, Project ID 390833453).

Data Availability

The data supporting the findings of this study are available from the corresponding author upon reasonable request. The numerical implementation was developed in Julia and is based in part on the open-source finite element package Ferrite.jl, including concepts from the topology optimization example available at `https://ferrite-fem.github.io/Ferrite.jl/stable/gallery/topology_optimization/`.

Author Contributions

S. Wolf developed the theoretical framework, performed the simulations, and wrote the manuscript. P. Junker supervised the research and revised the manuscript. All authors reviewed and approved the final manuscript.

Conflict of Interest

The authors declare that they have no known competing financial or non-financial interests that could have appeared to influence the work reported in this paper.

Abstract

Topology optimization in photonics is commonly formulated as a sequence of independent steps, including the definition of governing equations, adjoint problems, and heuristic material updates.
We show that this separation is artificial rather than fundamental. We derive a unified variational framework, in which the electrodynamic field equation, its adjoint counterpart, the balance of linear momentum, and the driving force governing the material distribution emerge as coupled stationarity conditions. In this formulation, the classical adjoint

structure arises naturally from the underlying variational principle, avoiding the need for separately derived sensitivity expressions.
The approach is applied to the design of a thermomechanically actuated photonic device, demonstrating that small temperature-induced deformations can trigger a substantial redistribution of the optical field. In particular, the optimized structure exhibits a clear switching behavior, where the dominant transmission channel shifts between the two output ports, with the majority of optical power redirected from the initial to the target port. This establishes a physically consistent and systematic foundation for multi-physics inverse design and demonstrates that thermomechanical actuation can be exploited through coupled geometric and material-induced modifications of the optical response.

1 Introduction

Photonic devices increasingly rely on inverse design strategies to exploit wave–matter interactions beyond intuitive geometries. In particular, topology optimization has enabled the realization of highly non-trivial structures such as metalenses with subwavelength focusing capabilities and wavelength-selective demultiplexers, demonstrating the potential of algorithmic design in photonics [7–9, 12, 13, 15, 16, 18, 24, 25, 27, 29, 30, 32, 34, 47].
Despite these advances, conventional formulations of photonic topology optimization remain inherently fragmented. The governing field equations, the adjoint problem, and the evolution of the material distribution are typically introduced as separate constructs, rather than arising from a common physical principle. While this separation is often manageable for purely electromagnetic problems, it becomes increasingly restrictive in multi-physics settings, where electromagnetic, mechanical, and thermal effects are strongly coupled.
At the same time, optical switching mechanisms inherently rely on such multi-physical interactions [3–6, 26, 37, 39, 40]. Switching behavior may arise from geometric reconfiguration, as in MEMS-based devices [11, 31, 36], or from modifications of the electromagnetic material response, such as thermo-optic or electro-optic effects [6, 10, 14, 26, 41]. These mechanisms are often strongly coupled and highly sensitive to small changes in geometry or material properties, making systematic design approaches essential.
In this work, we establish a unified variational framework for photonic topology optimization in which electromagnetic fields, mechanical deformation, and material evolution are derived simultaneously from a single action functional. Within this formulation, the state equation, its adjoint counterpart, and the driving force governing the material distribution emerge as coupled stationarity conditions, replacing the conventional sequence of objective definition, adjoint construction, and sensitivity analysis by a single physically consistent principle.
The proposed approach builds on thermodynamic topology optimization [20–22] and its recent extensions to photonics [44, 45]. Earlier work has demonstrated that variational formulations can be extended to incorporate electrodynamics and thermomechanical effects within a continuum-mechanical setting [45]. Furthermore, the integration of reciprocal formulations based on Betti's theorem has enabled the consistent definition of objective functionals for electromagnetic systems [43]. In addition, a quantitative comparison with classical adjoint-based topology optimization has been reported in [44], demonstrating comparable performance while highlighting the structural advantages of the variational formulation.
The present contribution unifies and extends these developments into a single framework that explicitly accounts for thermomechanical coupling within photonic topology optimization, thereby enabling the consistent treatment of multi-physics interactions within a unified variational setting.
Based on this formulation, we demonstrate that thermomechanical actuation can be exploited

to control electromagnetic wave propagation. In particular, we show that small temperature-induced deformations can trigger a pronounced redistribution of the optical field, enabling switching behavior that arises directly from the coupled physics.
For clarity and computational efficiency, the formulation is presented in a two-dimensional setting with out-of-plane polarization, allowing the electromagnetic problem to be expressed in terms of the vector potential. The fields are defined on the reference configuration and consistently coupled to the mechanical deformation via the deformation gradient. The material distribution is described by a density field augmented by regularization and penalization terms to ensure manufacturable designs.

2 Unified Variational Formulation of Coupled Electrodynamic–Mechanical Systems

2.1 Action Functional

Photonic topology optimization is formulated within a unified variational framework. In contrast to conventional approaches, both the governing physical equations and the evolution of the material distribution are derived from a single action functional.
The formulation is restricted to a resting, charge-free, two-dimensional setting with out-of-plane polarization of the electromagnetic field. This reduction provides an efficient scalar representation in terms of the out-of-plane component of the vector potential while preserving the essential wave-physical features of the coupled problem.
The system is entirely governed by the action functional

$$\mathcal{A}[\mathbf{A}_1, \mathbf{A}_2, \mathbf{u}, \chi, \Xi].$$

The functional depends on the following five independent variables:

- The vector potential $\mathbf{A}_1$ (in the reference configuration) describes the electromagnetic field oriented in the out-of-plane direction, while varying in the xy-plane.
- The vector potential $\mathbf{A}_2$ represents the adjoint field and shares the same properties as $\mathbf{A}_1$.
- The displacement field $\mathbf{u}$ describes the mechanical deformation of the domain.
- The density variable $\chi \in [0, 1]$ represents the material distribution, where $\chi = 0$ denotes void and $\chi = 1$ solid.
- The auxiliary field Ξ is obtained from a Poisson equation and penalizes isolated material islands in the evolution equation for χ.

The electric field in reference configuration $\mathbf{E}$ is given by the time derivative of the vector potential

$$\mathbf{E} = -\dot{\mathbf{A}}.$$

As the system is at rest, the total and partial time derivatives coincide. Likewise, the magnetic flux density follows from the curl of the vector potential

$$\mathbf{B} = \nabla_{\mathbf{X}} \times \mathbf{A}.$$

By expressing the electromagnetic fields in terms of the vector potential $\mathbf{A}$, Gauss's law for magnetism and Faraday's law are satisfied by definition. The vector potential is not uniquely

defined and therefore, a gauge condition must be imposed. Here, the Coulomb gauge is adopted, corresponding to the Lorenz gauge without scalar potential. This choice is consistent with the charge-free setting considered here, but does not constitute a general gauge prescription for arbitrary three-dimensional electrodynamic problems [1, 28, 35, 44]. The action is motivated by the original idea of Hamilton and extended in our previous works [42, 44, 45] by integrating the generalized four-momentum over the four-dimensional spacetime interval. It is given by

$$(1)\quad \mathcal{A}=\int_{t_0}^{t_1}\int_{\Omega} \underbrace{\mathbf{D}_1\cdot\mathbf{E}_2}_{\substack{\text{electric}\\ \text{cross energy}}} - \underbrace{\mathbf{B}_1\cdot\mathbf{H}_2}_{\substack{\text{magnetic}\\ \text{cross energy}}} + \underbrace{\mathbf{A}_1\cdot\mathbf{j}_2+\mathbf{A}_2\cdot\mathbf{j}_1}_{\text{reciprocal work}} - \underbrace{\Psi_{\mathrm{m}}}_{\substack{\text{mechanical}\\ \text{potential}}} - \underbrace{\Psi_{\mathrm{opt}}}_{\substack{\text{optimization}\\ \text{potential}}} + \underbrace{\Delta_{\chi}^{\mathrm{diss}}}_{\substack{\text{dissipation}\\ \text{function}}} \mathrm{d}V\,\mathrm{d}t.$$

In contrast to classical textbook formulations, the electromagnetic energy and work are not introduced in their standard form, but are constructed based on Betti's reciprocal theorem [42–44]. This approach describes the electromagnetic work exchanged between two systems, where an external current density $\mathbf{j}_1$ acting on the vector potential $\mathbf{A}_2$ is complemented by the reciprocal contribution. The same construction applies to the electromagnetic energy, resulting in symmetric interaction terms represented by the first two contributions of the functional.
The corresponding symmetric electric energy contributions are given by

- the internal work $\frac{1}{2}\mathbf{D}_2\cdot\mathbf{E}_1$, associated with the electric field $\mathbf{E}_1=-\dot{\mathbf{A}}_1$ acting on the dielectric displacement $\mathbf{D}_2=\varepsilon_0\varepsilon_{\mathrm{r}}J\mathbf{C}^{-1}\cdot(-\dot{\mathbf{A}}_2)$,
- and the internal work $\frac{1}{2}\mathbf{D}_1\cdot\mathbf{E}_2$, associated with the electric field $\mathbf{E}_2=-\dot{\mathbf{A}}_2$ acting on the dielectric displacement $\mathbf{D}_1=\varepsilon_0\varepsilon_{\mathrm{r}}J\mathbf{C}^{-1}\cdot(-\dot{\mathbf{A}}_1)$.

Herein, the vacuum permittivity is denoted by ε_0, while the relative permittivity is given by $\varepsilon_r=1+\varrho\chi_{\mathrm{e}}+i\alpha_{\mathrm{d}}\varrho(1-\varrho)$, depending on the interpolated material distribution ϱ and the electric susceptibility χ_{e}. The deformation is characterized by the deformation gradient $\mathbf{F}=\mathbf{I}+\nabla_{\mathbf{X}}\mathbf{u}$, its determinant J, and the right Cauchy–Green tensor $\mathbf{C}=\mathbf{F}^{\top}\cdot\mathbf{F}$.
The second term in (1) represents the magnetic counterpart $\mathbf{B}_1\cdot\mathbf{H}_2$ with the constitutive relation $\mathbf{H}=\frac{1}{\mu_0 J}\mathbf{C}\cdot\mathbf{B}$. The mechanical response is described by a Neo-Hookean free energy

$$\Psi_M=(((1-\kappa)\varrho)+\kappa)\left(G\left(\frac{1}{2}\mathrm{tr}(\mathbf{C}_{\mathrm{el}})-2-\log(J_{\mathrm{el}})\right)+\frac{\Lambda}{2}\left(\log(J_{\mathrm{el}})\right)^2\right)$$

based on the multiplicative decomposition $\mathbf{F}=\mathbf{F}_{\mathrm{el}}\cdot\mathbf{F}_{\mathrm{th}}$. The thermal expansion is modeled by an exponential approach $\mathbf{F}_{\mathrm{th}}=\mathbf{I}\exp(\alpha_\theta\Delta\theta)$ [46]. To promote binary designs, a smoothed Heaviside projection is applied,

$$\varrho(\chi)=\frac{\tanh(\zeta\xi)+\tanh(\zeta(\chi-\xi))}{\tanh(\zeta\xi)+\tanh(\zeta(1-\xi))},$$

where ζ controls the slope and ξ the threshold. Additionally, an artificial damping term controlled by α_{d} penalizes intermediate densities. The optimization process is governed by the potential

$$\begin{aligned}\Psi_{\mathrm{opt}}[\chi,\Xi]=&\underbrace{\gamma\chi+\lambda\left(h(\chi)-v_0\Omega\right)}_{\text{constraint part}}+\underbrace{\frac{1}{2}\beta\|\nabla_{\mathbf{X}}\chi\|^2}_{\text{regularization part}}\\&+\underbrace{\chi p_0(\mathrm{sign}(\Xi)-1)-\lambda_\Xi\|\nabla_{\mathbf{X}}\Xi\|^2-\Xi(\mathrm{sign}(\chi-0.5)-1)}_{\text{penalization part}}.\end{aligned}$$

The first term containing the Karush–Kuhn-Tucker parameter γ enforces $\chi \in [0,1]$, while the second term with the Lagrange multiplier λ, restricts the material volume fraction to v_0. The regularization term with the parameter β controls the minimum structural length scale and suppresses checkerboarding. Furthermore, p_0 controls the penalization strength and λ_Ξ acts as a heat transfer coefficient. Since dissipative processes cannot be represented by a potential, the dissipation function is modeled by $\Delta_\chi^{\text{diss}} := \frac{1}{2}\eta\dot{\chi}^2$ where η governs the rate of the density evolution and is critical for convergence. Furthermore, the variational framework can be consistently extended to include thermal quantities, whereby stationarity with respect to the temperature field θ yields the associated heat equation [19, 42, 45].

2.2 Governing Equations

In order to derive the system of governing equations, Hamilton's principle is applied by requiring stationarity of the action functional from Equation (1) with respect to the three independent variables, given in formulas as

$$\delta\mathcal{A} = \delta_{\mathbf{A}_1}\mathcal{A} + \delta_{\mathbf{A}_2}\mathcal{A} + \delta_{\mathbf{u}}\mathcal{A} + \delta_\chi\mathcal{A} + \delta_\Xi\mathcal{A} = 0.$$

The first two governing equations constitute the core of the approach. They form a coupled adjoint system derived from a single action functional; their structural similarity reflects this common origin, while their distinction enables a consistent sensitivity formulation.

$$\delta_{\mathbf{A}_1}\mathcal{A} = \int_{t_0}^{t_1}\int_\Omega -\mathbf{H}_2 \cdot \delta(\nabla_{\mathbf{X}} \times \mathbf{A}_1) - \mathbf{D}_2 \cdot \delta\dot{\mathbf{A}}_1 + \mathbf{j}_2 \cdot \delta\mathbf{A}_1 \mathrm{d}V\mathrm{d}t = 0 \tag{2}$$

$$\delta_{\mathbf{A}_2}\mathcal{A} = \int_{t_0}^{t_1}\int_\Omega -\mathbf{H}_1 \cdot \delta(\nabla_{\mathbf{X}} \times \mathbf{A}_2) - \mathbf{D}_1 \cdot \delta\dot{\mathbf{A}}_2 + \mathbf{j}_1 \cdot \delta\mathbf{A}_2 \mathrm{d}V\mathrm{d}t = 0 \tag{3}$$

These equations constitute the weak form of Ampère's circuital law and are readily implemented in a finite element framework. Applying Ohm's law $\mathbf{j} = \sigma J\mathbf{C}^{-1} \cdot \mathbf{E} + \mathbf{j}_{\text{ex}}$ and employing the exponential approach $\mathbf{A}_i = \tilde{\mathbf{A}}_i \mathrm{e}^{i\omega t}$ and $\mathbf{j}_{\text{ex}} = \tilde{\mathbf{j}}_{\text{ex}}\mathrm{e}^{i\omega t}$ yields the equations for the time-independent amplitudes $\tilde{\mathbf{A}}_1$ and $\tilde{\mathbf{A}}_2$.

The deformation state enters the governing equations through $\mathbf{C}$ and follows from the balance of linear momentum, obtained by variation with respect to $\mathbf{u}$:

$$\delta_{\mathbf{u}}\mathcal{A} = \int_\Omega \mathbf{P} : \delta\nabla_{\mathbf{X}}\mathbf{u}\,\mathrm{d}V = 0. \tag{4}$$

Electromagnetic body forces are neglected, as they are negligible compared to mechanical forces in photonic applications [42]. Furthermore, $\mathbf{P} = \partial\Psi_{\text{M}}/\partial\mathbf{F}$ denotes the first Piola–Kirchhoff stress tensor arising from the Helmholtz free energy.

The evolution equation follows directly from the stationarity condition with respect to the design variable, eliminating heuristic update schemes and ensuring that the material evolution arises consistently from the same action functional, yielding

$$\delta_\chi\mathcal{A} = \int_\Omega \left(-\tau + \eta\dot{\chi} - \beta\nabla_{\mathbf{X}}^2\chi + \gamma + \frac{\partial\varrho}{\partial\chi}\lambda - p_0(\text{sign}(\Xi) - 1)\right)\delta\chi\mathrm{d}V = 0 \tag{5}$$

The quantity $\tau = -\varepsilon_0 \frac{\partial \varepsilon_r(\chi)}{\partial \chi} \mathbf{E}_1^* \cdot \mathbf{C}^{-1} \cdot \mathbf{E}_2$, defines the driving force, where $\mathbf{E}_1$ and $\mathbf{E}_2$ are the solutions of the two coupled electromagnetic equations derived above, forming the state–adjoint pair, and thereby recovering the classical sensitivity formulation of topology optimization. For the purpose of optimization, the scalar quantity

$$\Pi = \int_\Omega \mathbf{D}_1 \cdot \mathbf{E}_2 \mathrm{d}V$$

is introduced as the global optimization potential, analogous to the objective functional in classical topology optimization.

To ensure numerical stability, only positive contributions are considered, accompanied by a suitable scaling of η and β. The term $p_0(\mathrm{sign}(\Xi) - 1)$ penalizes isolated material islands and is obtained from the stationarity condition with respect to Ξ itself

$$\delta_\Xi \mathcal{A} = \int_\Omega \left(\lambda_\Xi \nabla_{\mathbf{X}} \Xi \cdot \delta \nabla_{\mathbf{X}} \Xi + (\mathrm{sign}(\chi - 0.5) - 1)\delta\Xi\right) \mathrm{d}V = 0. \tag{6}$$

By choosing $\lambda_\Xi = \lambda_{\Xi_0}(\mathrm{sign}(\chi - 0.5))$, the Ξ-field propagates only through the connected regions where $\chi > 0.5$. Isolated material islands, being disconnected from the main structure, are naturally excluded from this flow. To facilitate the removal of Ξ, regions with $\chi < 0.5$ are defined as sinks.

All governing equations, including the adjoint system and the evolution equation, thus follow consistently from a single action functional.

3 Variational Topology Optimization Enables Thermomechanical Optical Switching

3.1 Problem Setup and Numerical Implementation

The proposed variational formulation yields both the governing equations and the material evolution. In the following, its capabilities are demonstrated on a thermomechanically actuated photonic device. The presented example is based on a demultiplexer, a standard benchmark in photonic topology optimization, which routes light of different wavelengths from a single input to multiple outputs.

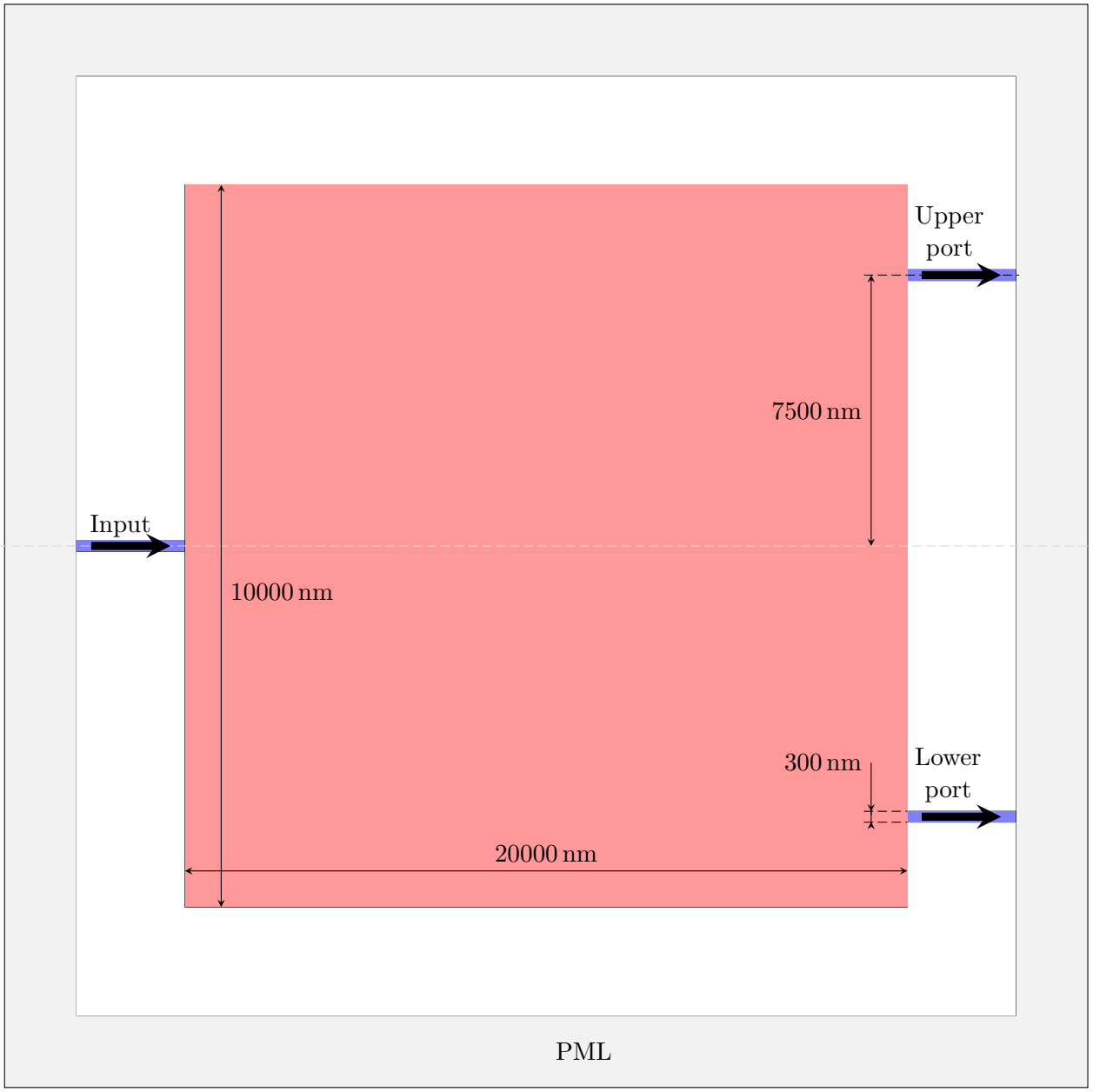

Figure 1: Computational domain. The design region is shown in red, the surrounding air domain in white, and the input/output regions in blue. The outer frame represents the perfectly matched layer (PML).

In the present study (Figure 1), this configuration is extended to a thermomechanically actuated switch, where a temperature change of $\Delta\theta = 400\,\mathrm{K}$ induces a deformation that redirects the optical signal of a single wavelength of $\lambda_0 = 1550\,\mathrm{nm}$ induced at the input from the upper to lower port. The induced electromagnetic waves are represented by Dirichlet boundary conditions of the form $\tilde{\mathbf{A}}_i = \exp\left[((y - y_0)/\Delta y)^2\right]$.

The solid material is modeled as silicon with an electrical susceptibility that varies with temperature, given by $\chi_\mathrm{e} = 11.098$ at $\Delta\theta = 0\,\mathrm{K}$ and $\chi_\mathrm{e} = 11.813$ at $\Delta\theta = 400\,\mathrm{K}$, reflecting the thermo-optical response of the material [14]. Geometric changes due to thermal expansion are treated separately through the mechanical deformation. The mechanical properties are simplified by assuming a constant Young's modulus $E = 1.3 \times 10^5\,\mathrm{N/nm^2}$ and a Poisson ratio $\nu = 0.27$. The coefficient of thermal expansion is set to $\alpha_\theta = 3.7 \times 10^{-6}\,\mathrm{K^{-1}}$, leading to moderate deformations that are sufficient to induce the switching behavior. The structure is mechanically fixed at the

input-side support region. The computational domain is defined accordingly, with the topology optimization performed in the design region, while the surrounding domain represents air. The input and output regions are defined in silicon. The outer frame is equipped with a perfectly matched layer (PML) to model an effectively infinite domain [2, 33].

For each configuration, the electromagnetic fields are computed for forward (input-driven) and backward (output-driven) excitations. The resulting field solutions enter the evaluation of the driving force, requiring two coupled simulations per configuration.

The optimization problem is solved numerically using the Neighbored Element Method (NEM) implemented in Julia [17, 23].

The physical fields are obtained using a finite element formulation, while the density evolution is treated using a finite difference scheme with explicit Euler time integration. Convergence to a steady state of the optimization potential Π defines the final optimized design.

This formulation provides an efficient and memory-conserving implementation while maintaining high accuracy, as demonstrated in recent studies [38]. The overall procedure is summarized in Figure 2.

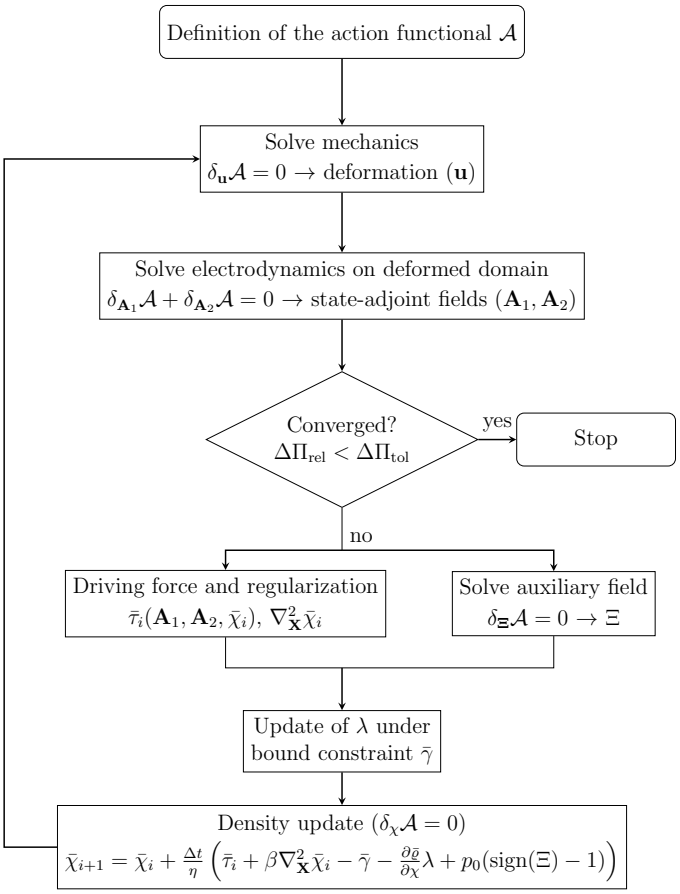

Figure 2: Program flow

3.2 Results and Discussion

The proposed framework is applied to the thermomechanically actuated switching device introduced in Section 3.1. The resulting optimized material distribution as well as the field amplitude are shown in Figure 3 for both the undeformed and deformed configurations.

The transmitted powers are evaluated at the output cross-sections and normalized by the input power. In the undeformed state (Figure 3, left), the optimized structure directs approximately 72% of the optical power into the upper output port, while 13% is transmitted to the lower port. Upon application of the external thermal load, the induced deformation only slightly alters the geometry (visualized with a scaling factor of 30), yet leads to a pronounced redistribution of the electromagnetic field. In the deformed configuration, approximately 75% of the optical power is redirected to the lower output port, while only 11% remains in the upper port.

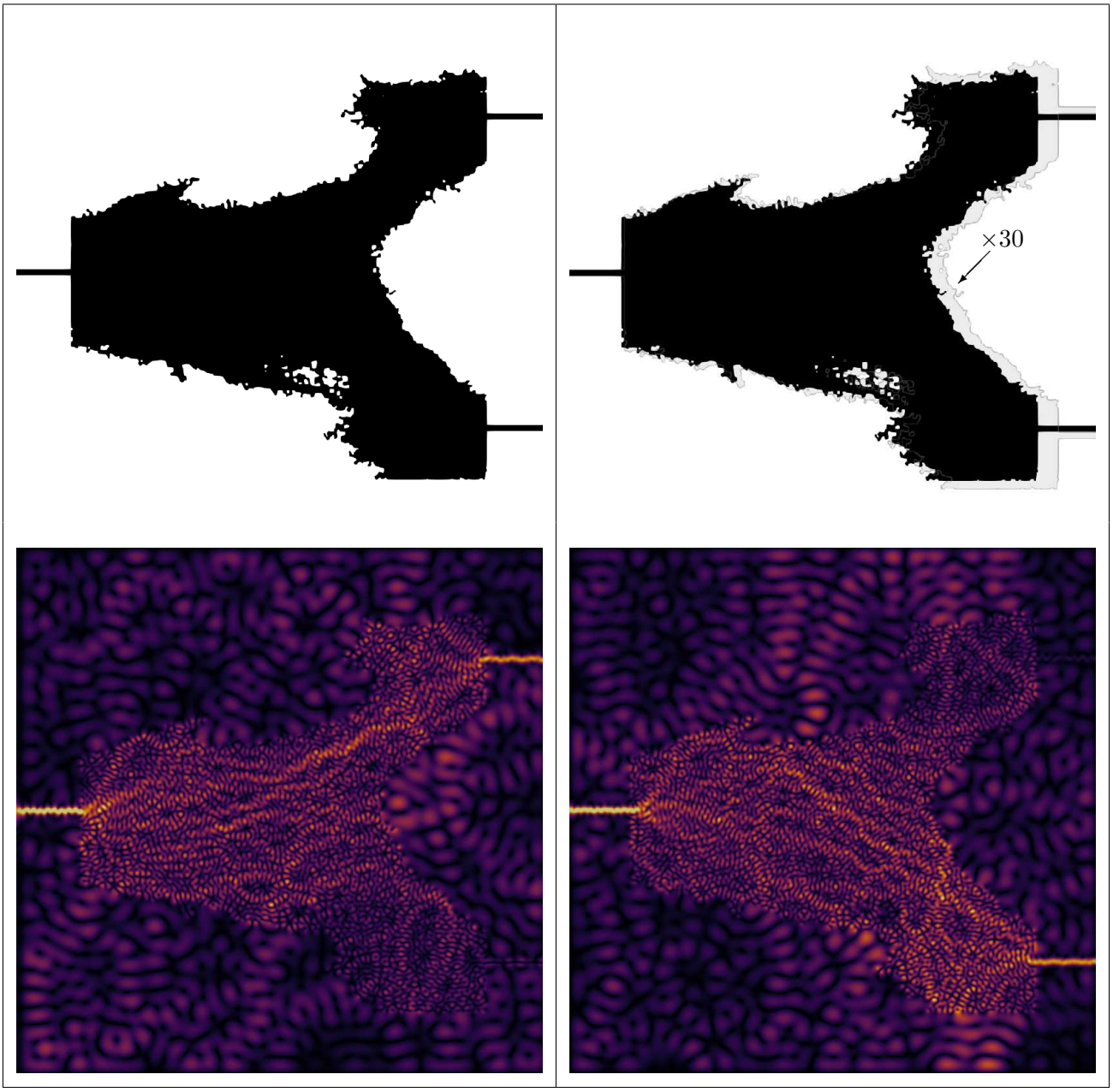

Figure 3: Optimized thermomechanically actuated optical switch. Top: material distribution; bottom: field magnitude. Left: undeformed configuration, with approximately 72% of the optical power transmitted to the upper port (13% to the lower port); right: deformed configuration, with approximately 75% transmitted to the lower port (11% to the upper port). The deformation is magnified by a factor of 30 for visualization. Discretization: 1200×1200. Parameters: $\beta = 0.04\,\mathrm{J/m}$, $(\eta = 15 + 15\zeta)\,\mathrm{J\,s/m^3}$, $\alpha_\mathrm{d} = 10$.

This corresponds to a distinct switching response between the two output channels, demonstrating that small thermally induced deformations can trigger a substantial reconfiguration of the optical power distribution.

The relatively large temperature change required to induce switching ($\Delta\theta = 400\,\mathrm{K}$) is primarily a consequence of the small coefficient of thermal expansion of silicon ($\alpha_\theta \approx 3.7 \times 10^{-6}\,\mathrm{K}^{-1}$), which limits the achievable geometric deformation. In the present study, silicon is deliberately chosen as a representative material system to isolate and demonstrate the underlying coupling mechanisms within the proposed variational framework, rather than to optimize actuation efficiency.

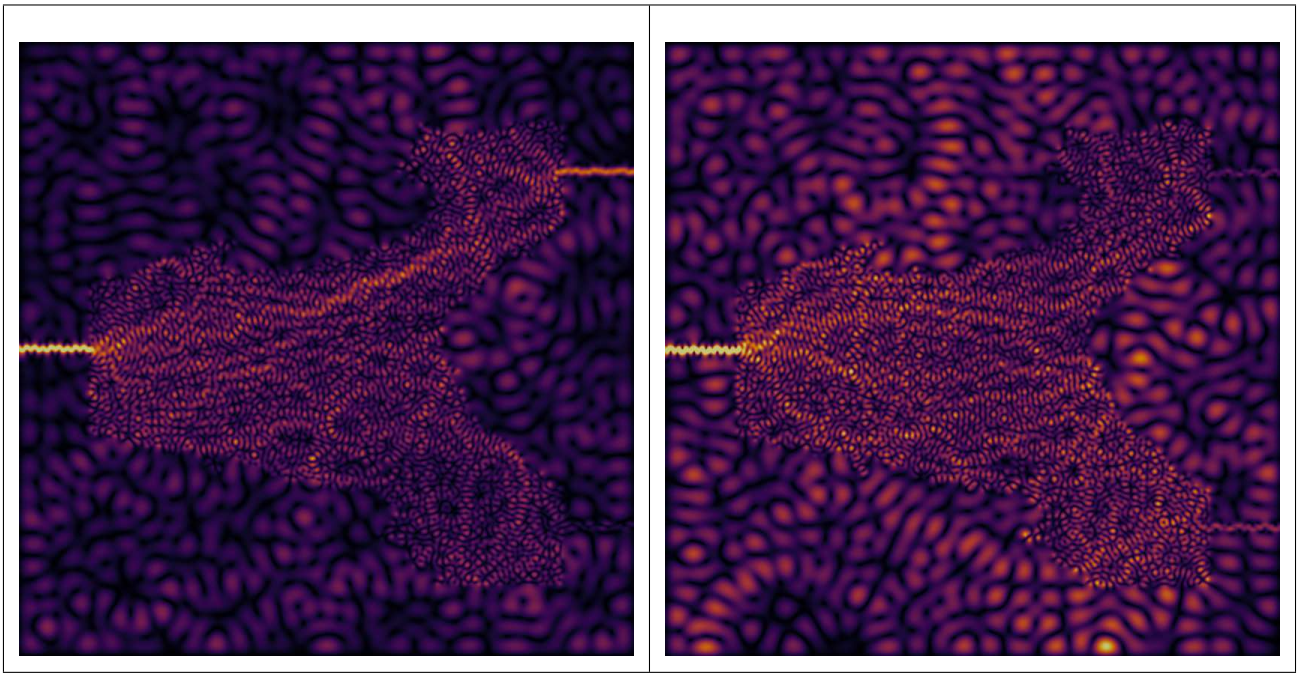

Figure 4: Geometric and material contributions to the switching behavior. Left: geometry-only response (62.72% upper, 10.91% lower); right: material-only response (23.14% upper, 35.87% lower).

To quantify the individual contributions to the switching response, Figure 4 shows the geometric and material-induced effects separately. The purely geometric case, considering only the deformation of the domain, does not switch the dominant output port, while the material-induced contribution, considering only the temperature dependence of the constitutive electromagnetic response, shifts optical power toward the lower port but remains insufficient to reproduce the full switching behavior shown in Figure 3. Thus, the observed switching response results from the coupled action of geometric reconfiguration and temperature-dependent material response. Despite this, the resulting deformation remains moderate, yet sufficient to induce a pronounced redistribution of the electromagnetic field. This demonstrates that the switching mechanism exploits the high sensitivity of the optical response to coupled thermomechanical changes in geometry and material properties.

Consequently, thermomechanical actuation constitutes an effective design mechanism within the proposed framework. While alternative material systems can significantly enhance actuation efficiency, they do not alter the fundamental mechanism demonstrated here. The optimized designs exhibit well-defined waveguiding structures with smooth transitions and no isolated material islands, indicating that the regularization and penalization terms effectively enforce manufacturable layouts. In particular, the density distribution converges to a nearly binary design, with less than $1.6 \times 10^{-4}\,\%$ intermediate material, despite the absence of classical filtering techniques, highlighting the robustness of the variational formulation.

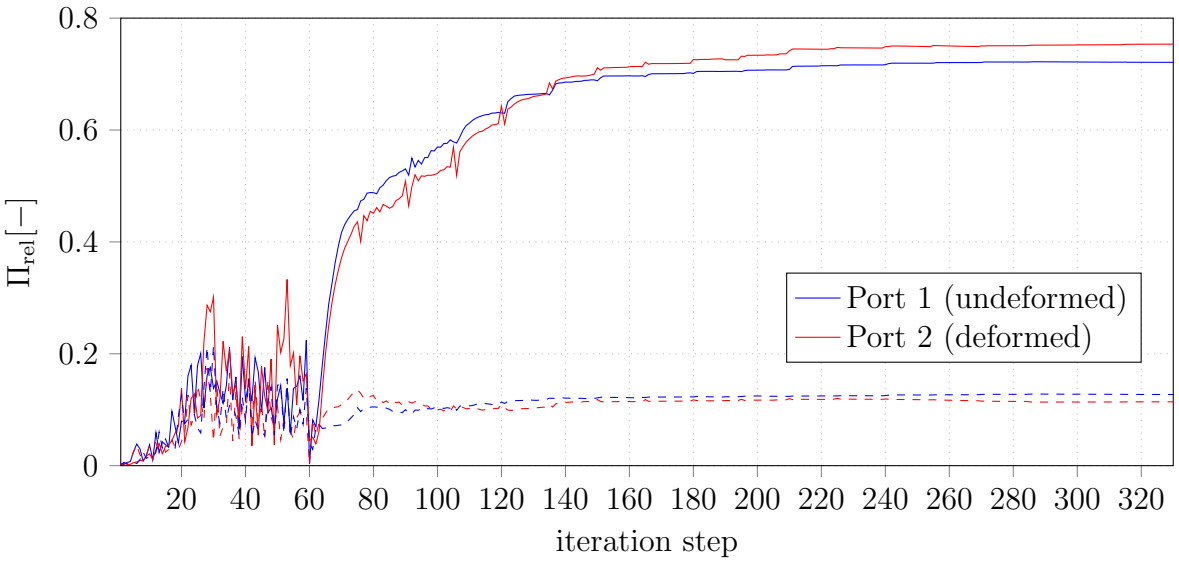

Figure 5: Evolution of the normalized optimization potential Π_{rel} for the upper and lower output port for α_{d} jumping at step 60 from 1 to 10 and a linear increasing numerical damping parameter of $\eta = 15 + 15\zeta$. Dashed lines indicate the corresponding non-activated ports.

The convergence behavior of the optimization process is shown in Figure 5. Prematurely large values of α_{d} were found to promote configurations that optically couple the input and output ports without forming a continuous material connection. To avoid such disconnected configurations, α_{d} is increased only after 60 iterations. Up to this point, the global optimization potential Π exhibits pronounced oscillations, whereas a stable convergence behavior is observed thereafter. The subsequent increase in the slope of the Heaviside function introduces occasional small fluctuations; however, these rapidly decay, and the overall convergence remains unaffected. The final design is obtained once the convergence criterion $\Delta\Pi_{\mathrm{rel}} < \Delta\Pi_{\mathrm{tol}}$ is satisfied.
In contrast to conventional photonic topology optimization approaches, where the adjoint problem and corresponding sensitivities are introduced as external constructs, the present formulation derives them directly from the variational structure. The driving force for the material evolution emerges naturally from the stationarity conditions of the action functional. This leads to a unified and thermodynamically consistent optimization process, in which all governing equations are derived from a single action functional by variation.
These results demonstrate that the proposed framework enables the design of thermally actuated photonic devices in a consistent and physically interpretable manner, opening new possibilities for the development of adaptive optical components.

4 Conclusion

We establish a unified variational framework for photonic topology optimization in which electrodynamics, mechanics, and material evolution are consistently coupled through a single action functional. Within this formulation, the governing field equations, their adjoint counterparts, and the driving forces for the material distribution emerge simultaneously as stationarity conditions. This replaces the conventional decomposition into physical modeling, adjoint construction, and heuristic design updates by a single physically grounded principle.
This shift has direct implications for multi-physics inverse design. By embedding the material evolution within the same variational structure as the underlying fields, the optimization process becomes intrinsically consistent with the governing physics. The resulting framework retains the

computational structure of state–adjoint methods, but removes the need to introduce sensitivities as external constructs, instead deriving them directly from the action functional.

On this basis, we demonstrate that thermomechanical actuation provides an effective and robust mechanism to control electromagnetic wave propagation. Temperature-induced deformations are used to induce a pronounced redistribution of the optical field, enabling switching behavior that arises directly from the coupled physics rather than from externally imposed design constraints. This establishes a route towards adaptive photonic devices in which mechanical and thermal effects are exploited as primary design variables.

Beyond the specific example considered here, the proposed formulation provides a general foundation for variationally consistent multi-physics topology optimization. It opens the possibility to systematically design reconfigurable photonic systems in which geometry, material, and fields evolve within a single, physically interpretable framework. This perspective shifts topology optimization from a purely numerical procedure to a physically grounded variational design principle.

References

[1] Matthias Bartelmann, Björn Feuerbacher, Timm Krüger, Dieter Lüst, Anton Rebhan, and Andreas Wipf. *Theoretische Physik 2 | Elektrodynamik*. Springer Berlin Heidelberg, Berlin, Heidelberg, 2018.

[2] Jean-Pierre Berenger. A perfectly matched layer for the absorption of electromagnetic waves. *Journal of Computational Physics*, 114(2):185–200, October 1994.

[3] Wim Bogaerts, Daniel Pérez, José Capmany, David A. B. Miller, Joyce Poon, Dirk Englund, Francesco Morichetti, and Andrea Melloni. Programmable photonic circuits. *Nature*, 586(7828):207–216, October 2020.

[4] Max Born. *Optik: Ein Lehrbuch der Elektromagnetischen Lichttheorie*. Springer Berlin Heidelberg, Berlin, Heidelberg, 1965.

[5] Max Born and Emil Wolf. *Principles of Optics: 60th Anniversary Edition*. Cambridge University Press, 7th edition, December 2019.

[6] Xiaojun Chen, Jiao Lin, and Ke Wang. A Review of Silicon-Based Integrated Optical Switches. *Laser & Photonics Reviews*, 17(4):2200571, April 2023.

[7] Rasmus E. Christiansen and Ole Sigmund. Compact 200 line MATLAB code for inverse design in photonics by topology optimization: tutorial. *Journal of the Optical Society of America B*, 38(2):510, February 2021.

[8] Rasmus E. Christiansen and Ole Sigmund. Inverse design in photonics by topology optimization: tutorial. *Journal of the Optical Society of America B*, 38(2):496, February 2021.

[9] Lianhong Dong, Weijie Kong, Changtao Wang, Guoyu Luo, Mingbo Pu, Xiaoliang Ma, Xiong Li, and Xiangang Luo. Inverse design of sub-diffraction focusing metalens by adjoint-based topology optimization. *New Journal of Physics*, 25(10):103026, October 2023.

[10] Matt Eichenfield, Jasper Chan, Ryan M. Camacho, Kerry J. Vahala, and Oskar Painter. Optomechanical crystals. *Nature*, 462(7269):78–82, November 2009.

[11] Carlos Errando-Herranz, Alain Yuji Takabayashi, Pierre Edinger, Hamed Sattari, Kristinn B. Gylfason, and Niels Quack. MEMS for Photonic Integrated Circuits. *IEEE Journal of Selected Topics in Quantum Electronics*, 26(2):1–16, March 2020.

[12] Jonathan A. Fan. Freeform metasurface design based on topology optimization. *MRS Bulletin*, 45(3):196–201, March 2020.

[13] A. R. Gersborg and O. Sigmund. Maximizing opto-mechanical interaction using topology optimization. *International Journal for Numerical Methods in Engineering*, 87(9):822–843, September 2011.

[14] Gorachand Ghosh. Temperature dispersion of refractive indices in crystalline and amorphous silicon. *Applied Physics Letters*, 66(26):3570–3572, June 1995.

[15] Emadeldeen Hassan and Antonio Calà Lesina. Topology optimization of dispersive plasmonic nanostructures in the time-domain. *Optics Express*, 30(11):19557, May 2022.

[16] Tyler W. Hughes, Momchil Minkov, Ian A. D. Williamson, and Shanhui Fan. Adjoint Method and Inverse Design for Nonlinear Nanophotonic Devices. *ACS Photonics*, 5(12):4781–4787, December 2018.

[17] Dustin R. Jantos, Klaus Hackl, and Philipp Junker. An accurate and fast regularization approach to thermodynamic topology optimization. *International Journal for Numerical Methods in Engineering*, 117(9):991–1017, March 2019.

[18] J.S. Jensen and O. Sigmund. Topology optimization for nano-photonics. *Laser & Photonics Reviews*, 5(2):308–321, March 2011.

[19] Philipp Junker and Daniel Balzani. An extended Hamilton principle as unifying theory for coupled problems and dissipative microstructure evolution. *Continuum Mechanics and Thermodynamics*, 33(4):1931–1956, July 2021.

[20] Philipp Junker and Daniel Balzani. A new variational approach for the thermodynamic topology optimization of hyperelastic structures. *Computational Mechanics*, 67(2):455–480, February 2021.

[21] Philipp Junker and Klaus Hackl. A variational growth approach to topology optimization. *Structural and Multidisciplinary Optimization*, 52(2):293–304, August 2015.

[22] Philipp Junker and Klaus Hackl. A discontinuous phase field approach to variational growth-based topology optimization. *Structural and Multidisciplinary Optimization*, 54(1):81–94, July 2016.

[23] Philipp Junker, Stephan Schwarz, Dustin R. Jantos, and Klaus Hackl. A fast and robust numerical treatment of a gradient-enhanced model for brittle damage. *International Journal for Multiscale Computational Engineering*, 17(2):151–180, 2019.

[24] Chanik Kang, Chaejin Park, Myunghoo Lee, Joonho Kang, Min Seok Jang, and Haejun Chung. Large-scale photonic inverse design: computational challenges and breakthroughs. *Nanophotonics*, 13(20):3765–3792, August 2024.

[25] Mohammadreza Khorasaninejad, Wei Ting Chen, Alexander Y. Zhu, Jaewon Oh, Robert C. Devlin, Charles Roques-Carmes, Ishan Mishra, and Federico Capasso. Visible Wavelength Planar Metalenses Based on Titanium Dioxide. *IEEE Journal of Selected Topics in Quantum Electronics*, 23(3):43–58, May 2017.

[26] Joo Hwan Ko, Young Jin Yoo, Yubin Lee, Hyeon-Ho Jeong, and Young Min Song. A review of tunable photonics: Optically active materials and applications from visible to terahertz. *iScience*, 25(8):104727, August 2022.

[27] Christopher M. Lalau-Keraly, Samarth Bhargava, Owen D. Miller, and Eli Yablonovitch. Adjoint shape optimization applied to electromagnetic design. *Optics Express*, 21(18):21693, September 2013.

[28] L. D. Landau and E. M. Lifshits. *The classical theory of fields*. Number v. 2 in Course of theoretical physics. Pergamon Press, Oxford ; New York, 4th rev. english ed edition, 1975.

[29] Zin Lin, Victor Liu, Raphael Pestourie, and Steven G. Johnson. Topology optimization of freeform large-area metasurfaces. *Optics Express*, 27(11):15765, May 2019.

[30] Abdullah Maher and Mohamed A. Swillam. All dielectric highly efficient achromatic metalens using inverse design optimization. *Scientific Reports*, 13(1):18827, November 2023.

[31] Leonardo Midolo, Albert Schliesser, and Andrea Fiore. Nano-opto-electro-mechanical systems. *Nature Nanotechnology*, 13(1):11–18, January 2018.

[32] Sean Molesky. Inverse design in nanophotonics. *NAtuRe PhotoNIcS*, 12, 2018.

[33] Frédéric Nataf. Absorbing boundary conditions and perfectly matched layers in wave propagation problems. In Ivan Graham, Ulrich Langer, Jens Melenk, and Mourad Sini, editors, *Direct and Inverse Problems in Wave Propagation and Applications*, pages 219–232. DE GRUYTER, September 2013.

[34] Meiyan Pan, Yifei Fu, Mengjie Zheng, Hao Chen, Yujia Zang, Huigao Duan, Qiang Li, Min Qiu, and Yueqiang Hu. Dielectric metalens for miniaturized imaging systems: progress and challenges. *Light: Science & Applications*, 11(1):195, June 2022.

[35] Dietmar Petrascheck and Franz Schwabl. *Elektrodynamik*. Springer Berlin Heidelberg, Berlin, Heidelberg, 2019.

[36] Niels Quack, Alain Yuji Takabayashi, Hamed Sattari, Pierre Edinger, Gaehun Jo, Simon J. Bleiker, Carlos Errando-Herranz, Kristinn B. Gylfason, Frank Niklaus, Umar Khan, Peter Verheyen, Arun Kumar Mallik, Jun Su Lee, Moises Jezzini, Iman Zand, Padraic Morrissey, Cleitus Antony, Peter O'Brien, and Wim Bogaerts. Integrated silicon photonic MEMS. *Microsystems & Nanoengineering*, 9(1):27, March 2023.

[37] Graham T. Reed and C.E. Jason Png. Silicon optical modulators. *Materials Today*, 8(1):40–50, January 2005.

[38] Tobias Rudolf, Felix Klempt, Hüray Ilayda Kök, Meisam Soleimani, Dustin Roman Jantos, and Philipp Junker. Computational efficiency and accuracy of the Neighbored Element Method. *Finite Elements in Analysis and Design*, 249:104353, July 2025.

[39] M. A. Ruhul Fatin, Dusan Gostimirovic, and Winnie N. Ye. Reconfigurable optical logic in silicon platform. *Scientific Reports*, 14(1):5950, March 2024.

[40] Bahaa E. A. Saleh. *Fundamentals of photonics I: Optics/ Bahaa E.A. Saleh, Malvin Carl Teich*. Wiley series in pure and applied optics. Wiley, Hoboken, NJ, 3rd edition, 2019.

[41] R. Soref and B. Bennett. Electrooptical effects in silicon. *IEEE Journal of Quantum Electronics*, 23(1):123–129, January 1987.

[42] Sebastian Wolf. *On an Extended Hamilton Principle of Electromagnetism and its Application to Topology Optimization of Optical Devices*. PhD thesis, Garbsen : Institut für Kontinuumsmechanik, Leibniz Universität Hannover, 2026.

[43] Sebastian Wolf, Dustin R. Jantos, and Philipp Junker. Thermodynamic Topology Optimization of compliant mechanisms including a multi-objective approach to prevent one-node connections. *Structural and Multidisciplinary Optimization*, 69(2):32, February 2026.

[44] Sebastian Wolf, Dustin R. Jantos, and Philipp Junker. Topology optimization of photonics based on thermodynamically consistent variational principles. *Journal of the Optical Society of America B*, 43(3):516, March 2026.

[45] Sebastian Wolf and Philipp Junker. On an extended Hamilton principle for electro/magneto-thermo-mechanical materials with dissipative microstructure evolution. *Continuum Mechanics and Thermodynamics*, 37(3):49, May 2025.

[46] P. Wriggers, C. Miehe, M. Kleiber, and J. C. Simo. On the coupled thermomechanical treatment of necking problems via finite element methods. *International Journal for Numerical Methods in Engineering*, 33(4):869–883, February 1992.

[47] Jiaxin Zhang, Sirui Bi, and Guannan Zhang. A directional Gaussian smoothing optimization method for computational inverse design in nanophotonics. *Materials & Design*, 197:109213, January 2021.